

## Density Measurements of the Inner Shell Release

D. Haberberger, A. Shvydky, J. P. Knauer, S. X. Hu, S. T. Ivancic, J. Carroll-Nellenback, D. Cao, V. V. Karasiev,  
A. V. Maximov, V. N. Goncharov, and D. H. Froula

Laboratory for Laser Energetics, University of Rochester

The material release on the back side of a CH shell was probed at conditions relevant to inertial confinement fusion (ICF). The release was found to expand further with a longer scale length than that predicted by radiation-hydrodynamic simulations. The simulations show that a relaxation of the back side of the shell consistent with measurements explains the experimentally observed reduction in ICF implosion performance—specifically reduced areal density at peak compression.

While great progress has been made over recent years in ICF experiments,<sup>1</sup> achieving ignition conditions remains a grand challenge. In both direct- and indirect-drive approaches to fusion, a cold layer of deuterium–tritium (DT) fuel is compressed by material ablation to form a high-areal-density confinement around an igniting central hot spot. In both approaches, several shocks are launched through an outer solid-density fuel and into a central vapor region. Once the shock breaks through the inner surface into the central region, the fuel spherically converges to form a high-areal-density confinement. By limiting the amount of material and maintaining a low temperature inside the vapor region, the implosion can reach maximum convergence and the hot-spot temperature necessary for ignition.

One of the reasons for the underperformance in the recent experiments is attributed to a reduced areal density of the fuel; 20% deficiency has been reported for most of the implosions at the National Ignition Facility.<sup>2</sup> Several mechanisms could contribute to the reduction in shell convergence and therefore in areal density, including mixing of the ablator material into the fuel or mixing of the fuel into the central hot spot. In addition, inaccurate modeling of the material properties of fuel interacting with multiple strong shocks could lead to an underprediction of the mass expanding from the inner surface of the main shell by material release. Such a release is created as the first shock breaks out of the main fuel into the vapor region of the target. As subsequent shocks with increasing strengths are launched into the shell at the beginning of the implosion, they travel through the rarefaction formed by the earlier shocks. The rate of material release is determined by several factors, including sound speed, ion viscosity, and thermal conduction.

Experimental signatures of the driven shell dynamics are commonly used to test hydrodynamic simulations. In implosion experiments, x-ray backlighting or self-emission measurements are used to track the shell trajectory,<sup>3</sup> but they give no information about the low-density material release behind the shell since the low-density material does not attenuate the high-energy x-ray photons. Optical probing with a velocity interferometer system for any reflector (VISAR) has been used to track a shock moving through a transparent material or to measure when the shock breaks out into vacuum.<sup>4</sup> Although these measurements are very useful for studying the equation of state (EOS) in simulation codes, no information is gained about the profile of material release when the shock breaks through the shell because at this point the optical beam is absorbed near the critical plasma density of the rarefaction wave because of its reflection geometry.

In this research, the first direct measurements of the low-density plasma released from the back side of a laser-driven shell is presented. The low-density plasma (at  $10^{20} \text{ cm}^{-3}$ ) was measured to travel  $\sim 190 \mu\text{m}$  in front of the driven shell with a scale length that increased to a maximum to  $63 \mu\text{m}$  over 3 ns (Fig. 1). These observations are in contrast to hydrodynamic simulations that

show the plasma traveling  $\sim 80 \mu\text{m}$  away from the shell with a steep density gradient that increased to  $15 \mu\text{m}$  (Fig. 2). Further investigation uncovered the sensitivity of the inner shell expansion to the initial (before the shock breakout) CH density profile. By initiating the back side of the shell with a  $10\text{-}\mu\text{m}$  density gradient, release profiles matching those observed in the experiment were obtained. The more-rapid expansion results from enhanced heating of the lower-density material by the shock as it breaks out, causing a higher sound speed, and consequently, a faster post-shock expansion. This early relaxation of the CH shell boundary is consistent with estimations of preheat from x rays emanating from the hot coronal plasma. Implementing an expanded profile on the back side of the DT ice layer in direct-drive ICF implosion simulations shows a reduced convergence leading to an 18% lower areal density and a 17% smaller ion temperature.

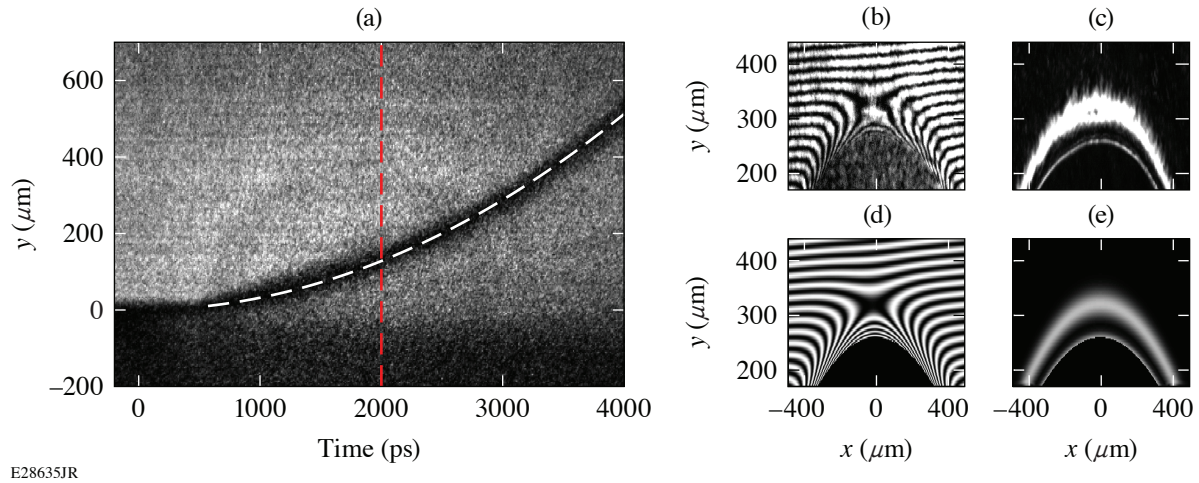


Figure 1

(a) The PJXI diagnostic measured the shell trajectory by tracking absorption of the Al He x rays traveling through the interaction region. The origins of the spatial and temporal axes represent the initial location of the center of the CH shell (spatial) at the beginning of the drive laser pulse (2% of rise, temporal). The  $4\omega$  probe diagnostic measures the density of the released plasma on the back side of the driven shell through (b) interferometry and (d) AFR at 2 ns after the drive. The synthesized response of the (c) interferometry and (e) AFR diagnostics that best match the corresponding measurements at 2 ns. The origin of the y axis corresponds to the position of shock ( $\sim 120 \mu\text{m}$ ) as measured by the radiography (dashed red line).

Figure 1(a) shows a radiograph where the shock is observed breaking out of the back side at  $t = 580 \pm 40$  ps. After this time, the shell trajectory was observed to accelerate at a near-constant acceleration of  $\sim 32 \mu\text{m}/\text{ns}^2$  (dashed white line) across  $\sim 540 \mu\text{m}$  over 4 ns. For this experimental setup, the 1.5-keV x rays provide an optimal peak absorption of  $\sim 70\%$ . The x-ray streak-camera diagnostic had a measured spatial resolution of  $20 \mu\text{m}$ , which was sufficient to track the position of the shell, although not small enough to resolve the expected shell thickness of 5 to  $7 \mu\text{m}$ .

To measure the density profile in the rarefaction wave, an 8-ps-FWHM-duration,  $4\omega$  (263-nm) probe beam was used to generate interferometry<sup>5</sup> [Fig. 1(b)] and angular filter refractometry<sup>6</sup> [AFR, Fig. 1(c)] data. The two diagnostics were used in conjunction to gain confidence in the measured plasma density profiles. The interaction was probed at four times with respect to the beginning of the drive beams (2% of rise): 1 ns, 2 ns (Fig. 1), 3 ns, and 4 ns. For the probe timing of 2 ns, the shell moved  $\sim 120 \mu\text{m}$  at the center of the laser spot [Fig. 1(a)]. Figure 1(b) shows the phase change accrued from propagating through the released plasma. A measurable phase change at the center of the shell is evident for distances greater than  $\sim 290 \mu\text{m}$ ; for positions less than this, the light was refracted outside of the collection optics. Refraction of the probe light from its propagation through this plasma resulted in the observation of two bands [Fig. 1(c)] of constant refraction angle corresponding to  $0.75^\circ$  (outer) and  $3^\circ$  (inner). The images were analyzed by simulating a synthetic interferogram and AFR image using an analytic function for the plasma density and iterating until the images converged to the measurements. A single exponentially decaying profile, with a transverse Gaussian function, was found to be adequate to reproduce the measurements. Other analytic profiles were tested and delivered very similar plasma profiles. The matched synthetic interferogram and AFR image for the 2-ns data are shown in Figs. 1(d) and 1(e), respectively, and correspond to a plasma density profile of  $n_e(x, y, z) = n_0 \exp[-y = L_y] \exp\left\{-\frac{(x^2 + z^2)}{[L_{\text{FWHM}}/2 \ln(2)]}\right\}$ , where  $n_0 = 3.6 \times$

$10^{21} \text{ cm}^{-3}$ ,  $L_y = 38 \text{ }\mu\text{m}$ , and  $L_{\text{FWHM}} = 340 \text{ }\mu\text{m}$ . Note, this profile is accurate only in the low-density region measured by the  $4\omega$  probe and is expected to strongly diverge from the actual plasma profile closer to the driven shell.

Figure 2 shows that the low-density plasma has expanded significantly farther than *LILAC*<sup>7</sup> radiation-hydrodynamic simulations predict. At the earliest measured time (1 ns), the low-density plasma is  $40 \text{ }\mu\text{m}$  in front of the predictions, while the position of the shell is in good agreement. Between 1 ns and 4 ns, the low-density (at  $10^{20} \text{ cm}^{-3}$ ) plasma is measured to have an average velocity of  $\sim 205 \text{ }\mu\text{m/ns}$ , while its scale length expanded from  $10 \text{ }\mu\text{m}$  to  $63 \text{ }\mu\text{m}$ . The average simulated expansion speed of  $145 \text{ }\mu\text{m/ns}$  at  $10^{20} \text{ cm}^{-3}$  was slower than the measurements, and the scale lengths increased from  $2 \text{ }\mu\text{m}$  to  $15 \text{ }\mu\text{m}$ , which are shorter than measured across the entire time span. This discrepancy was largely insensitive to the thermal transport and the EOS models used in the simulations. It was found in simulations that the position of the low-density plasma, as well as its scale length, significantly depends on the mass-density profile at the back surface of the CH shell right before the shock breaks out. The simulation results shown in Fig. 2 used an infinitely sharp boundary on the back side of the CH, as is typical in hydrodynamic simulations. These simulations significantly underestimate the plasma expansion at all times. When the back side of the CH target was relaxed over  $10 \text{ }\mu\text{m}$  (linear increase from zero to solid density prior to the shock breakout), the simulated trajectories are in excellent agreement with the measurements. The increased heating (from 20 eV to  $\sim 100 \text{ eV}$ ) that occurs from the shock propagating through the relaxed back side of the shell, results in a faster expansion and larger scale length than when the standard sharp interface is used. Note the trajectory of the shell was unchanged by this relaxation.

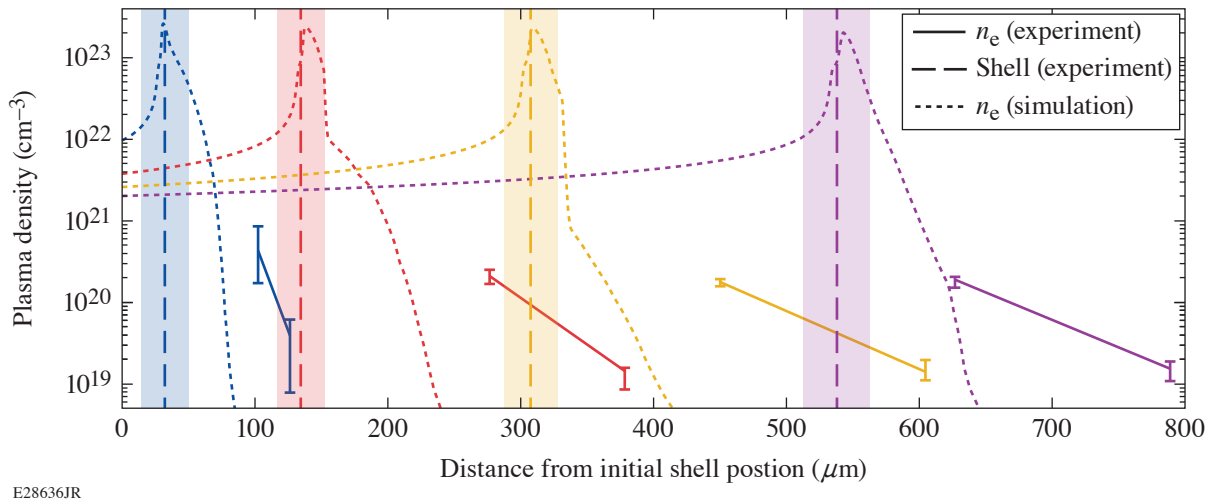


Figure 2

The measured (solid curves) and simulated (dotted curves) plasma density profiles at 1 ns (blue), 2 ns (red), 3 ns (yellow), and 4 ns (purple) are plotted. The vertical dashed lines are the peak shell position as measured by the PJXI diagnostic (with error bars shown by the shaded regions).

In summary, optical probing using interferometry and angular filter refractometry was used to study the material release from the shock breakout at conditions relevant to ICF implosions. It was observed that the position and scale length in the measured density range ( $10^{19}$  to  $10^{20} \text{ cm}^{-3}$ ) of the rarefaction wave strongly depends on the density profile at the back surface of the CH before the shock passes. To match the experimental data, simulations required a relaxation that results in a neutral-density gradient on the inner surface of the CH shell before the shock pass. This lower-density material is strongly heated by the passing shock, which causes it to expand more rapidly and have a longer scale length at later times. Radiation preheat by coronal x rays can cause such a relaxation of the back surface of the CH and formation of the density gradient. Simulations of direct-drive cryogenic implosions that enhanced the inner surface release consistent with these measurements show a significant reduction in target performance, including an 18% reduction in areal density, a 17% reduction in ion temperature, and more than a factor of 2 reduction in the neutron yield.

This material is based upon work supported by the Department of Energy National Nuclear Security Administration under Award Number DE-NA0003856, the University of Rochester, and the New York State Energy Research and Development Authority

1. S. Le Pape *et al.*, Phys. Rev. Lett. **120**, 245003 (2018).
2. D. S. Clark *et al.*, Nucl. Fusion **59**, 032008 (2018).
3. D. T. Michel *et al.*, Rev. Sci. Instrum. **83**, 10E530 (2012).
4. M. A. Barrios *et al.*, Phys. Plasmas **17**, 056307 (2010).
5. A. Howard *et al.*, Rev. Sci. Instrum. **89**, 10B107 (2018).
6. D. Haberberger *et al.*, Phys. Plasmas **21**, 056304 (2014).
7. J. Delettrez, Can. J. Phys. **64**, 932 (1986).